# Molecular Modeling Investigation of Free Volume Distributions in Stiff Chain Polymers with Conventional and Ultrahigh Free Volume: Comparison between Molecular Modeling and Positron Lifetime Studies

**Dieter Hofmann,*,† Maria Entrialgo-Castano,† Adrien Lerbret,‡ Matthias Heuchel,† and Yuri Yampolskii§**

*GKSS Research Center, Institute of Chemistry, Kantstr. 55, D-14513 Teltow, Germany; ISMANS, 44 avenue FA Bartholdi, 72000 LE MANS, France; and A. V. Topchiev Institute of Petrochemical Synthesis, Russian Academy of Sciences, 29 Leninsky Pr., 119991 Moscow, Russia*

*Received July 10, 2003; Revised Manuscript Received August 28, 2003*

ABSTRACT: The present paper deals with a molecular modeling-based characterization of the distribution of free volume in a number of different stiff chain glassy polymers including ultrahigh free volume and conventional materials. The free volume distribution was analyzed for the validated packing models and compared with respective positron annihilation data (if available). It will be shown that the molecular modeling approach permits a more detailed insight into free volume distributions. There the observed distributions reach from more or less symmetric monomodal (with maximum probability at free volume element radii of about 3 Å) via monomodal distributions with extended tails toward larger radii up to distinctly bimodal distributions with a tendency toward a continuous nanoporous free volume phase besides "conventional", free volume organized in isolated holes of radii up to a few angstroms. The described sequence roughly corresponds to the trend of measured permeabilities for small molecules in the investigated materials.

## 1. Introduction

The free volume distribution in amorphous polymers is of paramount importance for their transport behavior toward small- and medium-sized penetrant molecules. There are several experimental methods to characterize the free volume of a polymer, with the positron annihilation lifetime spectroscopy (PALS) as the most common one.[1−3] As could be shown in a foregoing paper,[4] molecular modeling can be an interesting alternative for the characterization of free volume size distributions.

In this paper, we discuss the results of molecular modeling for a relatively large group of polymers with widely varying free volume and transport properties. It includes the following: an ultrahigh free volume polymer poly[1-(trimethylsilyl)-1-propyne] (PTMSP) in original and the aged state; a chemically similar conventional glassy polymer poly[vinyltrimethylsilane] (PVTMS); two highly branched polyacetylenes with extremely bulky side groups, poly[1-phenyl-2-[*p*-(triphenylsilyl)-phenyl]acetylene] (PPhSiDPA) and poly[1-phenyl-2-[*p*-(triisopropylsilyl)phenyl]acetylene] (PPrSiDPA); and at last two ultrahigh free volume perfluorinated polymers—amorphous Teflons, AF1600 (65 mol % 2,2-bis(trifluoromethyl)-4,5-difluoro-1,3-dioxole [BDD] and 35 mol % tetrafluoroethylene [TFE]), and AF2400 (87 mol % BDD and 13 mol % TFE). All these materials are amorphous and glassy at room temperature. Scheme 1 shows their structures, and Table 1 presents some of their physical properties: density, glass transition temperature $T_g$, and oxygen permeability. Solubility coefficients for several gases will be considered later in comparison with the simulated values.

Molecular modeling techniques have been widely used over the past decade to get a deeper insight into the structure and the transport behavior of nonporous amorphous polymer membranes. General results of these investigations can be found for example in a number of reference and feature articles.[5−7]

## 2. Modeling Details

For each of the polymers at least three (in some cases up to eight) independent atomistic bulk models were realized employing the amorphous cell module of the InsightII/Discover software of Accelrys Inc.[8] The applied basic techniques of packing and equilibration are completely described elsewhere.[4,7,9,10] However, a summary of the procedures applied will follow below. The COMPASS force field[11,12] of Accelrys Inc. was utilized for all models.

Summarizing details on the simulated packing models (e.g., chain length and resulting packing cell sizes) are given in Table 2. It should be mentioned that the average cell sizes employed in this work having, typically, more than 8000 atoms are larger than common in the literature. The aims of using so large cells were to improve the statistics of the derived free volume data.

In the following the general conditions applied for generating the packing models shall be described in more detail. Special considerations for some of the investigated polymers follow afterward. For PTMSP and PVTMS, which both do not contain aromatic or other cyclic groups, initial bulk polymer packing cells were created utilizing the amorphous cell module of the InsightII/Discover software of Accelrys Inc.[8] The polymer chains were grown at 303 K under periodic boundary conditions. The volume of the respective basic cell was in theses cases chosen in a way reproducing the respective experimentally obtained macroscopic density (cf. Table 2). The packing procedure in these cases and

† GKSS Research Center, Institute of Chemistry.
‡ ISMANS.
§ Russian Academy of Sciences.
* Corresponding author: e-mail Hofmann@gkss.de.

10.1021/ma034971l CCC: $25.00 
Published on Web 09/30/2003

**Scheme 1. Chemical Structures of the Investigated Polymers**

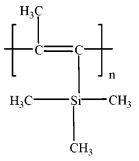

PTMSP

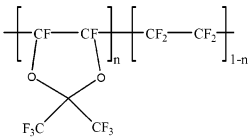

n=0.65 Teflon AF1600

n=0.83 Teflon AF2400

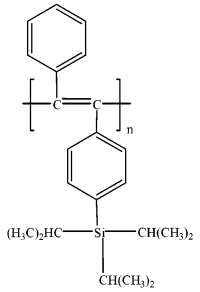

PPrSiDPA

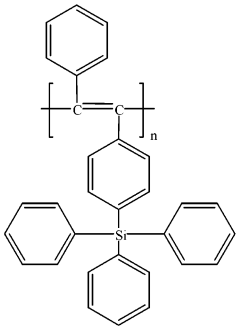

PPhSiDPA

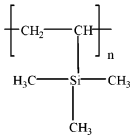

PVTMS

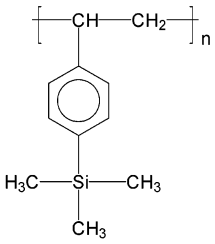

PTMSS

**Table 1. Some Physical Properties of the Polymers**

| polymer | volumetric density (g cm$^{-3}$) | $T_g$ (°C) | typical measured oxygen permeability (barrers) |
|---|---|---|---|
| PTMSP | 0.7−0.8 (refs 47, 48) | >290 (ref 48) | 9000 (ref 16) |
| PTMSP-095 (aged) | 0.9−0.95 (refs 23, 49) | >200 (ref 23) | 140 (ref 23) |
| Teflon AF2400 | 1.7 (ref 50) | 240 (ref 50) | 1140 (ref 25) |
| Teflon AF1600 | 1.8 (ref 50) | 160 (ref 50) | 170 (ref 25) |
| PPrSiDPA | 1.038 (ref 16) | >270 (ref 16) | 230 (ref 16) |
| PPhSiDPA | 1.121 (ref 16) | >430 (ref 16) | 12 (ref 16) |
| PVTMS | 0.88 (ref 51) | 140−150 (ref 51) | 44 (ref 51) |
| PTMSS | 0.965 (ref 27) | 135 (ref 27) | 56 (ref 27) |

**Table 2. Simulation Data[a]**

| polymer | no. of repeat units | no. of atoms | density (g cm$^{-3}$) | av size of the periodic cell (Å) |
|---|---|---|---|---|
| PTMSP-095 | 499 | 9483 | 0.95 | 46.090 |
| Teflon AF2400 | 585 | 8803 | 1.75 | 49.828 |
| Teflon AF1600 | 700 | 8216 | 1.82 | 46.662 |
| PPrSiDPA | 150 | 8102 | 1.038 | 43.140 |
| PPrSiDPA-50 | 150 | 8102 | 1.038 | 43.140 |
| PPhSiDPA | 140 | 7982 | 1.121 | 44.896 |
| PVTMS | 500 | 8902 | 0.8826 | 45.517 |

[a]Respective data for PTMSP and PTMSS can be found in ref 4.

**Table 3. Scaling Factors of the Five-Step Equilibration Used for Packing Models**

| stage of equilibration | scaling factor for the torsion term | scaling factor for nonbonded interactions |
|---|---|---|
| 1 | $10^{-3}$ | $10^{-3}$ |
| 2 | $10^{-2}$ | $10^{-3}$ |
| 3 | 1 | $10^{-3}$ |
| 4 | 1 | $10^{-2}$ |
| 5 | 1 | 1 |

for other polymers utilizes the backbone conformation angle statistics which can be obtained from the applied force field (cf. ref 8). The resulting initial packing models were equilibrated using force field parameter scaling (cf. ref 7) according to the procedure outlined in Table 3. The individual stages lasted for 1000 fs with a time step of 0.2 fs and were always preceded by a short energy minimization of several hundred iterations.

**Catenation and Spearing Problem**. Since the repeat units of most of the investigated polymers contain ring structures, a technical problem occurs in the packing and equilibration process that is absent in the case of linear polymers with no cyclic structures. (cf. e.g. refs 7 and 14). For cyclo-linear systems, the packing algorithm may lead to artifacts of catenated rings (e.g., phenylene rings) or a spearing of side groups or backbone chains through ring substructures. Both effects are, of course, unacceptable and have to be avoided. To solve this technical problem, it is usually necessary to start modeling with a nonrealistically low initial packing density (typically 0.1 g/cm$^3$). However, for some polymers, such an approach alone did not lead to a complete disappearance of catenation and spearing events. Therefore, an alternative technique was chosen. First 200 methane molecules were placed in each packing cell. These objects served as obstacles preventing the respective growing polymer chains from ring catenations and spearings. Later, the obstacle molecules must be removed again. Then a polymer chain was allowed to grow in the respective periodic cell. At this stage, the initial densities were taken as 0.4 g/cm$^3$, whereas the final densities (cf. Table 2) matched ex-

**Table 4. Parameters of the Temperature Cycle Used To Further Equilibrate Packing Models**

| stage of equilibration | temperature (K) | time (ps) |
|---|---|---|
| 1 | 750 | 20 |
| 2 | 600 | 20 |
| 3 | 450 | 20 |
| 4 | 303 | 100 |

perimental values given in Table 1. It should be noted that other commercial software, like Cerius2 of Accelrys Inc., instead of using obstacle molecules to prevent catenations and spearings permit the application of pseudo-atoms in the centers of the critical ring structures. This is not possible with the InsightII software applied here. In addition, our approach to a certain extent mimics the processes occurring during the film formation for most of the polymers via evaporation or other types of removal of solvents.

As in the case of PTMSP and PVTMS, the resulting initial packing models were equilibrated using force field parameter scaling (cf. Table 3). 110 of the 200 methane molecules were then removed, and the resulting models were again equilibrated using the procedure described in Table 3. Then, the remaining methane molecules were finally eliminated, and the cell side length was reduced to account for the removal of the obstacle molecules. The final cell side lengths are given in Table 2. Then the third equilibration followed.

Afterward each packing model including those for PTMSP, and PVTMS was subjected to a 300 ps NVT-MD equilibration with a time step of 1 fs. Finally, an additional simulated annealing procedure (cf. Table 4) had to be applied for some of the models to achieve reasonable coincidence between simulated and measured solubility coefficients (see below).

**Polyacetylenes**. In modeling polyacetylens, the cis−trans ratios of the main chains had to be used as input parameters. In the calculations, we were eager to use the experimental values of these ratios. However, in the cases of polyacetylenes PPhSiDPA and PPrSiDPA (in contrast to PTMSP), no experimental results were available on the cis−trans ratio. Therefore, it was planned to realize different cis−trans ratios for the chains to be packed in a model and then to check which ratio would give best agreement between measured and simulated solubility data. For this purpose the respective repeat units were constructed in trans and cis configuration. Then first assuming the backbone double bonds are all trans, we simulated the chains with the Polymerizer module of the Accelrys software.[13] For PPhSiDPA the sterical hindrance between the bulky side groups was so severe that catenations between benzene rings occurred when the flexible conformation angles between each two repeat units were set to the default all trans value of 180°. A systematic trial and error procedure resulted, however, in 120° as possible inter-repeat-unit conformation angle which was used for the construction of the respective starting chains needed as topological templates for the subsequent chain packing procedure. Then further attempts were made to realize chains of different ratios of cis and trans conformers. Thus, for PPrSiDPA, the chains with 50% cis contents were easily realizable. For PPhSiDPA, on the other hand, despite numerous systematic attempts, the maximum content of cis conformers, which could be introduced in the linear (nonbranched) chains, was only 5%; at higher cis content a catenation of benzene rings occurs. This can be an indication that the underlying problems of sterical hindrance should also refer to the cis−trans configuration statistics of the real polymer. Because of this problem, for the further simulations of PPhSiDPA only 100% trans configurations were considered in preparing the packing models.

For polyacetylenes (PPhSiDPA and PPrSiDPA) 7−8 independent all-trans atomistic bulk models were realized in each case. In addition, for PPrSiDPA three 50% cis models were also constructed. They are labeled below as PPrSiDPA-50.

The first three packing models for the aged PTMSP-095 were prepared as described in ref 4 for as cast PTMSP except that a geometric density of 0.95 g/cm$^3$ instead of 0.75 g/cm$^3$ was applied. Another three "aged" packing models were obtained from the original PTMSP models with a density of 0.75 g/cm$^3$ via a simulated annealing/NPT-shrinking procedure as described in ref 7.

## 3. Comparison with Experiments

The results of computer modeling of free volume and its size distribution in the polymers under investigation were compared with experimental studies of free volume. The most widely accepted experimental technique for this purpose is the positron annihilation lifetime spectroscopy (PALS). However, the results of other, so-called probe methods (inverse gas chromatography (IGC), $^{129}$Xe NMR) will also be addressed. Experimental data based on the PALS studies of the polymers simulated in this work have been reported earlier.[3,15−17] The IGC method was applied to investigate the free volume of amorphous Teflons AF earlier. The results of the study of these polymers using the $^{129}$Xe NMR technique have been reported in ref 18.

## 4. Results and Discussion

**4.1. Validation of the Packing Models.** The aim of this work was to analyze free volume and its distribution as obtained via the packing models. A convenient and widely accepted way to validate the packing models obtained is a comparison of the predicted and experimental values of the solubility coefficients of small molecules in a polymer. Here we check the quality of the obtained equilibrated packing models by a comparison the predicted and experimental solubility coefficients for four gases ($H_2$, $O_2$, $N_2$, $CH_4$). Here the solubility coefficient is defined as the amount of gas (in cm$^3$) under standard conditions (STP) solved per unit volume of the polymer (in cm$^3$) at 1 bar of outside gas pressure. The experimental values $S_{exp}$ were taken from the literature.[17,25,31,49,51,52] The results are presented in Table 5. The systematic particle insertion part of the Gusev−Suter method[20−22] was applied to obtain the needed simulated solubility coefficients $S_{sim}$ for these gases.

A remark should be made concerning the aged PTMSP (PTMSP-095). There is a wide variety of possible aging mechanisms of this polymer; they depend on the specific conditions under which the process of aging proceeds (see review by Nagai et al.[24]).

1. Physical aging (density relaxation). This is the fastest process; it can proceed even in a vacuum. Apparently, this mechanism should be responsible for the formation of the structure considered in the PTMSP-095 packing models.

2. Aging due to irreversible absorption of some impurities from atmosphere or in exploitation. It can

**Table 5. Comparison of Simulated and Experimental Solubility Coefficients (in $cm^3$ (STP)/$cm^3$ bar)[a]**

| polymer | method | $H_2$ | $O_2$ | $N_2$ | $CH_4$ |
|---|---|---|---|---|---|
| PTMSP-aged | sim | 0.3 | 1.8−2.0 | 0.9−1.4 | 3.3−4.9 |
| | exp | | | | |
| PVTMS | sim | 0.10−0.11 | 0.43−0.44 | | 0.84−0.89 |
| | exp[35,51] | 0.08 | 0.41−0.44 | 023−0.30 | 0.76−0.99 |
| PPrSiDPA | sim | 0.1−0.2 | 0.9−1.2 | 0.6−0.8 | 2.1−2.8 |
| | exp[49] | | 2.5 | 1.4 | 4.7 |
| PPrSiDPA-50 | sim | 0.2 | 0.9−1.2 | 0.6−0.8 | 2.1−2.8 |
| | exp[49] | | 2.5 | 1.4 | 4.7 |
| PPhSiDPA | sim | 0.13−0.17 | 1.2−1.5 | 0.9−1.2 | 3.4−4.5 |
| | exp[49] | | 0.75 | 0.41 | 1.8 |
| AF2400 | sim | 0.3 | 2.1 | 1.4−1.5 | 4.4−4.6 |
| | exp[17,31,52] | | 0.9 | 0.6−0.8 | 1.2−1.3 |
| AF1600 | sim | 0.3 | 2.0 | 1.3−1.4 | 4.3−4.4 |
| | exp[17,25,31,52] | | 0.7−0.9 | 0.6−0.8 | 0.95−1.2 |

[a] Respective results for PTMSP and PTMSS can be found in ref 4.

be, for instance, plasticizer or some vapors (e.g., oil vapor from a vacuum pump).

3. "Chemical" aging caused by oxidation reactions, e.g., by reactions with oxygen.[23,24] It is likely that this process is accelerated by traces of catalysts in polymers.

In this regard, a very wide range of transport parameters for small molecules are reported for "aged" samples in the literature. Thus, the PTMSP-095 models created at a density of 0.95 g/$cm^3$ only illustrate a possible result of just long time physical aging (0.95 g/$cm^3$ is at the upper end of reported geometric densities for aged PTMSP). We did not find any direct measurements of solubility of oxygen in completely physically aged PTMSP, so no validation can be given for this system.

Let us outline briefly the basics and limitations of the solubility prediction part of the Gusev−Suter method. In this approach, a systematic particle insertion technique is used to estimate solubilities of small gas molecules and positions of free volume elements. In addition, the energy barriers (or diffusion jump probabilities) between adjacent portions of free volume can be also found. The method is based on the assumption that the polymer networks do not have to undergo structural relaxation (e.g., resulting from torsion transitions) to accommodate an inserted particle. Therefore, this simulation technique is basically restricted to relatively small molecules (often just up to $N_2$).

When considering the results shown in Table 5, one should bear in mind that due to the inherently nonequilibrium state of glassy polymers possible deviations of predicted and experimental solubility coefficients can be relatively high for these materials. Some additional reasons for relatively large deviations are caused by peculiarities of the prediction procedure: even relatively small errors of the insertion energy, which are determined by the quality of a respective model and the applied force fields, may lead to rather high errors in $S_{sim}$. Therefore, it is generally accepted that a coincidence between measured and simulated solubility coefficients within a factor of 3 can be regarded as reasonable (cf. e.g. ref 5).

The results shown in Tables 5 indicate that in most cases the simulated values $S_{sim}$ do not deviate from $S_{exp}$ more than by a factor of 2. In some cases the agreement is even better. A reasonable agreement is also observed for a larger molecule of $CH_4$ for which not all the prerequisites of the Gusev−Suter model are satisfied. This implies that the amount and distribution of the free volume, which are of interest here, should be representative for the "real" materials. No systematic differences between the coincidence of measured and simulated solubility coefficients could be noted both for 100% trans and 50% cis PPrSiDPA models. This indicates that, at least from the modeling point of view, a wide variation of cis−trans ratios is possible for this material.

**4.2. Qualitative and Quantitative Characterization of Free Volume**. Previously we have considered[4] the ultrahigh free volume polymer, PTMSP. It has been shown that this polymer contains regions of high segmental packing density, where the free volume distribution resembles that in conventional glassy polymers. On the other hand, computer modeling revealed an existence of rather large voids having a tendency to form a partly continuous hole phase with lateral void widths between about 5 and 20 Å. It should be emphasized that under continuous phase we will understand a presence of such free volume clusters that allow transport of small penetrant molecules like hydrogen or oxygen without overcoming considerable energy barriers.

Figure 1 shows a qualitative "visual" impression of the free volume distributions for single (typical) packing models of each of the polymers studied. For comparison, a model of "nonaged" PTMSP is given as well.[4] The figure presents in each case a series of approximately monatomic layers (slices) cut perpendicular to the respective *z*-axis with the distance between successive slices of about 3 Å. It is obvious that a group of high free volume, high permeability polymers (PTMSP, AF2400, AF1600, and even PTMSP-aged) are distinguished by the presence of two qualitatively different environments for small penetrants. On one hand, they contain the regions of high segmental packing density where the free volume distribution resembles that in conventional glassy polymers. On the other hand, these polymers reveal rather large voids with a tendency to a partly continuous hole phase (here the applied periodic boundary conditions are to be considered) with lateral void widths between ca. 5 and 20 Å. A closer look shows that the tendency toward a continuous hole phase of rather large lateral dimensions is most pronounced for PTMSP, followed in decreasing order by AF2400, AF1600, and aged-PTMSP. It can be reminded that this is exactly the order of decreasing the gas permeability and diffusivity in these polymers.

However, in the cases of less permeable polymers, PVTMS, PPrSiDPA, and PPhSiDPA, the respective free volume distribution comprises smaller microvoids, and there is no indication of a continuous hole phase. This result seems to be surprising for the two polyacetylenes with very bulky side groups. It indicates that bulkiness

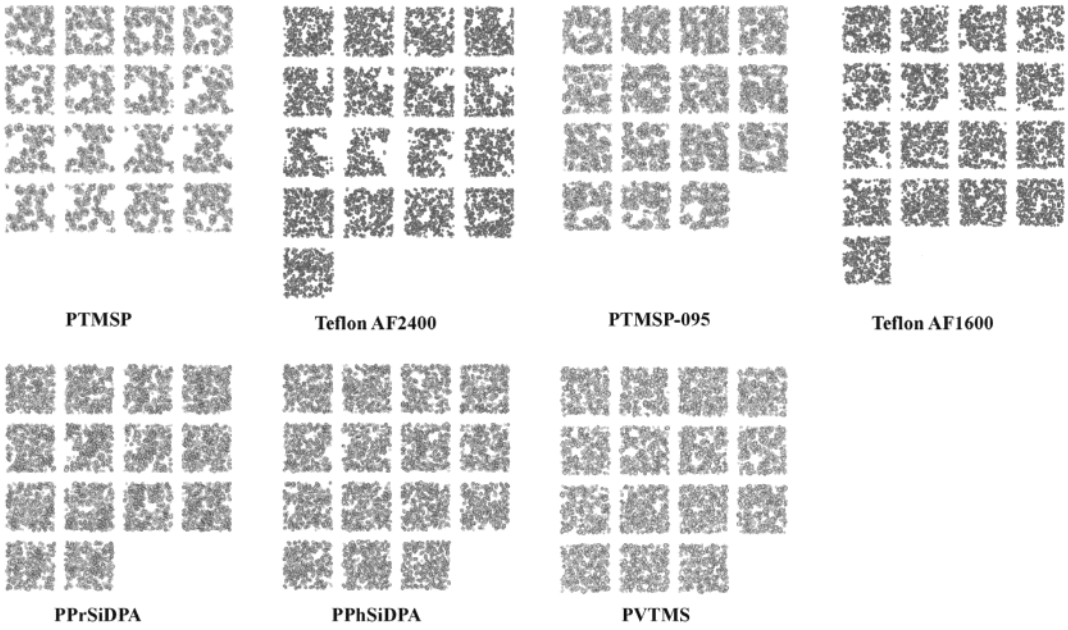


**Figure 1.** Qualitative "visual" impression of the free volume distributions for typical packing models of each of the polymers studied. The figure presents in each case a series of approximately monatomic layers (slices) cut perpendicular to the respective *z*-axis with the distance between successive slices of about 3 Å (cf. Table 2 for the lateral dimensions). The PTMSP picture was already published as one part of Figure 1 of ref 4.

of side groups alone in glassy polymers cannot serve as a prerequisite of "open" structure of free volume. This is consistent with observations that many other polyacetylenes with bulky substituents show rather low gas permeability.[24]

The following procedure was developed to get a more quantitative description of the free volume distributions. The polymer chains of the respective packing models were represented by atomic hard spheres with the van der Waals radii of the respective atoms (C, 1.55 Å; H, 1.10 Å; O, 1.35 Å; F, 1.30 Å; Si, 2.20 Å). To determine the free volume distributions and the fractional accessible free volume (FAV), the cubic packings were overlaid by a three-dimensional grid with a grid size $\delta$ of 0.7 Å. Two particles were selected as the probes: positronium (radius 1.1 Å) and oxygen molecule (1.73 Å). At every grid point, it was then tested if a hard sphere with the radius of the respective probe molecule would overlap with the hard spheres at the atom positions of the polymer. All grid points showing overlap with the polymer matrix are subsequently called *occupied* while those without overlap are called *free*. The free volume accessible for a type of probe molecule was then estimated by the ratio of number of free grid points to the total number of grid points. The overall FFV is the fractional free volume sensed by a probe with the radius of 0 Å. It was determined by geometric calculations of the volume occupied by the polymer chain segments and subtracting this value from the overall volume of the respective model. Table 6 shows respective values for FAV sensed by positronium and oxygen molecules plus the overall FFV of the investigated polymers (that is FAV for probes having size close to zero). The FAV and FFV values in Table 6 account only the volume accessible for the center of the respective probe molecule; i.e., they are not subjected to the corrections described below.

While conventional glassy polymers presented in the lower part of Table 6 show overall FFV values in the range 30−35%, these values increase up to nearly 50%

**Table 6. Fractional Accessible Volume (FAV) Determined Geometrically for the Center of Probe Molecules with Different Radius $r_{Test}$ (Refs Cf. Table 1)**

| | fractional accessible vol (FAV) for probes with radii $R_i$ (Å) | | | typical measd $O_2$ permeability |
|---|---|---|---|---|
| polymer | 1.73 ($O_2$) | 1.10 (o-Ps) | 0.00 (FFV) | (barrers) |
| PTMSP | 0.113 | 0.180 | 0.471 | 9000 |
| Teflon AF2400 | 0.057 | 0.104 | 0.474 | 1140 |
| Teflon AF1600 | 0.022 | 0.062 | 0.453 | 170 |
| PVTMS | 0.003 | 0.018 | 0.339 | 44 |
| PTMSS | <0.001 | 0.009 | 0.336 | 56 |
| aged-PTMSP | 0.016 | 0.050 | 0.335 | |
| PPhSiDPA | 0.006 | 0.024 | 0.314 | 12 |
| PPrSiDPA-50 | 0.007 | 0.024 | 0.293 | 230 |
| PPrSiDPA | 0.006 | 0.022 | 0.292 | 230 |

for the ultrahigh free volume materials. Here it should be noted that the zero radius FFV values account even the most minute spaces not filled by polymer atoms. For membrane applications, however, the free volume accessible for a given penetrant radius (FAV) is, of course, more important. This observation can partly explain rather poor correlations[28] with FFV found using the Bondi procedure,[29] which includes the whole void distribution. It is seen that when the size of a probe increases the FAV values dramatically decrease.

An attentive analysis of Table 6 enables us to make several interesting observations. An increase in permeability of the polymers is accompanied by increases in both FFV and FAV values. The found FFV values can be compared with commonly made assessment of "Bondi" free volume.[29] The FFV values obtained by computer simulation in this work are by a factor 1.3−1.6 larger than Bondi FFV calculated using the formula

$$\mathrm{FFV} = 1 - 1.3V_w/V_{sp} \qquad (1)$$

where $V_w$ is the sum of van der Waals volumes of atoms with the repeat unit and $V_{sp}$ is specific volume of polymers equal to reciprocal density $1/\rho$. Presumably, the universal packing coefficient 1.3 accepted in the

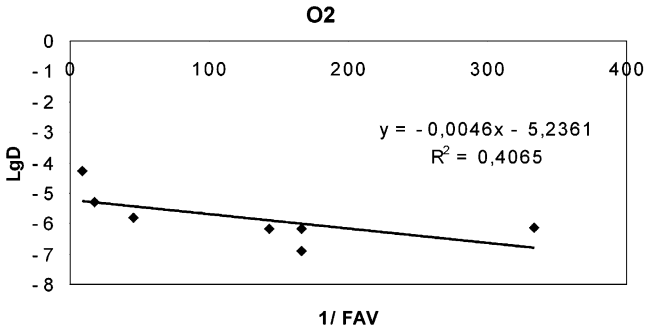


**Figure 2.** Experimental diffusion coefficients of oxygen ($cm^2$ $s^{-1}$) vs 1/FAV.

Bondi method does not correspond to actual packing densities of polymer chains in the glassy state.

It is common to consider the correlation of permeability coefficients $P$ of a gas with free volume or FFV of different polymers. Strictly speaking, this approach based on the free volume model is not completely correct because $P = DS$, where $D$ and $S$ are diffusion and solubility coefficients, respectively, and the free volume model is applicable only to $D$. The results of this work allow one, for the first time, to make an attempt to correlate the diffusion coefficients of oxygen $D(O_2)$ with FAV sensed by oxygen molecule. Such correlation is shown in Figure 2. The diffusion coefficients were taken from the literature.[16,17,25,26,30,31] The deviations from assumed linear dependence

$$\log D(O_2) = A - B/\mathrm{FAV}(O_2) \qquad (2)$$

are rather great. This indicates that other factors beyond overall free volume accessible to $O_2$ molecules should be taken into account when considering different polymers. It can be nanostructure (topology) of free volume (see below) and the role of processes that take place in densely packed matrix surrounding free volume elements as has been discussed elsewhere.[7,32,33] The correlation shown in Figure 2 is of the type "one gas−different polymers". It will be interesting to use the same method for calculation of FAV for the system "one polymer−different gases", which is for the same polymer structure and by varying the size of diffusing probe molecule. An attempt to obtain such correlations was undertaken in another work.[34]

Let us consider how FAV depends on the size of probe molecules. Figure 3 indicates that the FAV values in different polymers are inversely proportional to the squared radius of the probes. This dependence is consistent with fulfillment of eq 2 and a well-known dependence[35]

$$\log D = A' - B'd^2 \qquad (3)$$

where $d$ is the diameter of the diffusing gas molecules.

There is another way to relate the calculated FFV and FAV values to the gas transport properties of polymers. It has been shown[15] that the size of free volume elements in glassy polymers correlates with the diffusion selectivity $\alpha_D$ defined as the slope ($-B'$) of the dependence given by eq 3. (Note that this more general definition of diffusion selectivity differs from the often applied definition via the ratio of diffusivities of two different penetrants in the same polymer.) On the other hand, the diffusion selectivity $\alpha_D$ can depend on the parameter d(FAV)/d$r$, which characterizes the variation

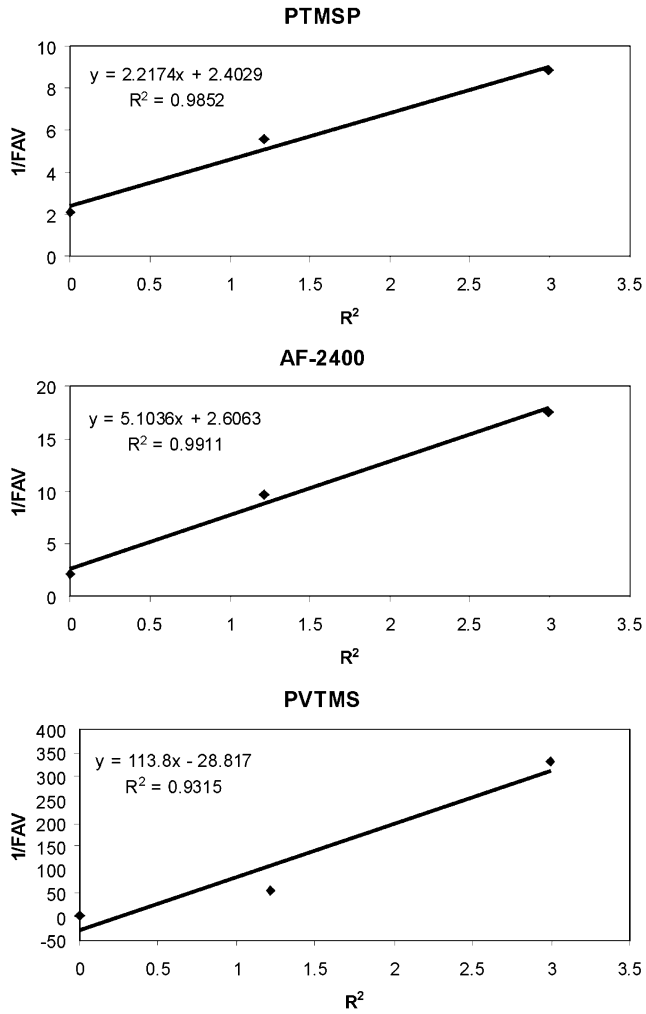


**Figure 3.** Correlation of FAV with squared probe radius $R$ in several polymers (the same correlations are valid for others).

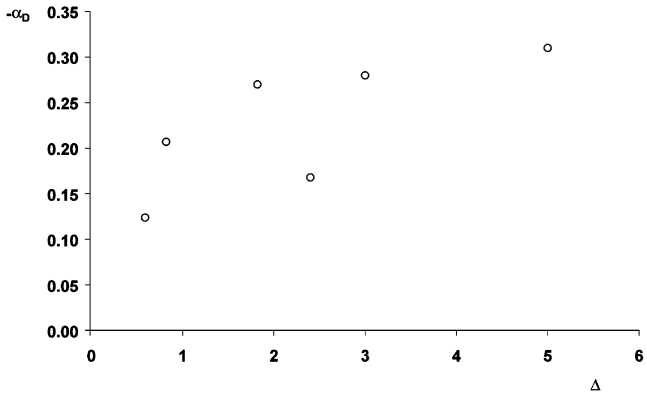


**Figure 4.** Correlation of the diffusion selectivity with the dimensionless selectivity Δ (cf. eq 4).

of FAV for the probes of different size. It is convenient to us this parameter in the dimensionless form

$$\Delta = [\mathrm{FAV(Ps)} - \mathrm{FAV}(O_2)]/\mathrm{FAV}(O_2) \qquad (4)$$

Figure 4 indicates that, indeed, such a dependence is fulfilled. The values of diffusion selectivity were taken from ref 15. It is clear that for polymers with low diffusion selectivity (e.g., PTMSP or AF2400) it is caused by relatively weak changes of the accessible free volume (FAV) when the size of the probe is changed. For conventional glassy polymers that are characterized by

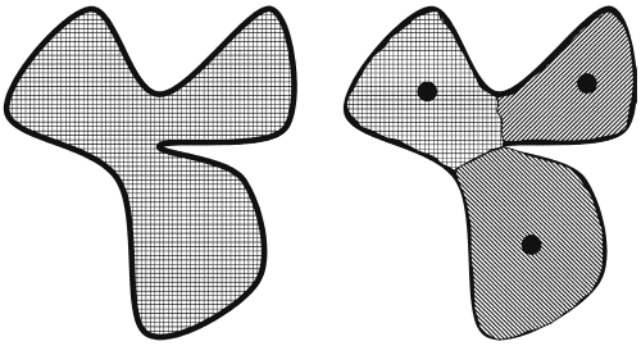

**Figure 5.** *V*_connect (left) and *R*_max (right) view on a large hole of complex topology.

greater size selective diffusion FAV changes stronger as a function of the probe size. In more quantitative manner it should be mirrored in size distribution of free volume elements as will be considered further in this work.

For finding a more detailed relationship between free volume properties and measured transport parameters, a more sophisticated description (the size distribution) of the free volume is advised. It is obvious that the resulting distributions should depend on the size of the probe particles which scan the free volume regions. The same should be true for the applied experimental methods for measurement of free volume Thus, the observed PALS spectra are supposed to be characterized by a cutoff radius of about 1.1 Å, which is the size of orthopositronium (o-Ps) atom.

Here only a brief description of the used methodology is given. A more extended consideration can be found in ref 4. The method utilizes information already obtained the determination of FFV described above, namely the calculation of the numbers of the cells, where the probe molecules inserted in the lattice are free or have an overlap with atoms of the polymer matrix. In interpreting the nanostructure of free volume elements, the two approaches should be considered.[4] Visualization of these approaches is shown as a sketch in Figure 5.

In the *R*_max approach, first, the shortest distance between each lattice point belonging to the free volume and an atom of the polymer matrix is calculated. Among these distances, local maxima are defined by calculating the related gradient. Then each grid point of the free volume regions is assigned to its nearest local maximum (simply speaking, the center of a distinct part of the free volume, i.e., the black dots in the right part of Figure 5), in which way individual holes are defined. This method may clearly divide elongated and frayed parts of free volume into more compact parts. A second approach (named *V*_connect) just utilizes simple topological connectivity criteria to group all nonoccupied cells of the probe molecule insertion grid to individual holes, which may be of more complex shape and of larger size (cf. left part of Figure 5).

Today, in the existing experimental probe methods for investigation of free volume, the probes of different size and shape (o-Ps atoms in the PALS method, Xe atoms in the $^{129}$Xe/NMR method, and organic molecules of different size in the IGC method) are used to scan free volume elements in polymers. However, it is difficult to judge whether they "see" large holes with complex topology or sets of smaller holes with more simple shape. One can assume an overlapping of these two extreme descriptions of the probing patterns. Hitherto, at least for ultrahigh free volume polymers like PTMSP, the *R*_max approach has given better agreement between modeled free volume distributions and those measured in the PALS experiments.[4]

In this work, we will perform a more systematic analysis of hole size distribution based on two probes (o-Ps and $O_2$) and compare the results of simulation with the data of several experimental probe methods.

In both approaches the number of lattice cells belonging to a hole times the volume of a $\delta^3$ cubicle was used as a measure for the volume of this hole accessible by the center of the test particle. The obtained volume of each hole is converted to an equivalent sphere, the radius of which could be taken as a measure for the average linear dimensions of the respective hole. But this would be only a measure for the size of the *accessible* volume with respect to the *center* of the test particle. (In the extreme case, i.e., a hole just of the size of the probe molecule, the volume of the test particle would be represented by the volume of a $\delta^3$ cubicle only. Similar less extreme problems occur in the surface region of any hole.) Thus, this simple approach would underestimate the volume of the hole which could be filled by probe molecules of certain size. To get a better estimate for this quantity, a correction was introduced. For every free grid point of a hole, an appropriate segment of volume of the probe sphere was added to the total volume of the hole depending on the number of occupied neighboring grid points. The correction was zero, when all neighbor sites of a the considered grid point were also unoccupied (nonsurface region of a hole), and it would be the total volume of the probe sphere, when the considered free site would be surrounded only by occupied grid points The introduction of this correction makes the results slightly different from those reported earlier[4] (cf. also below).

The resulting free volume distribution functions (percentage of the free volume organized in holes of a given size) from the V-connect approach (for o-Ps and $O_2$ probe cases) and the *R*_max technique (only for o-Ps) for the all investigated polymers are presented in Figures 6−8. For each polymer the distribution was determined from all available equilibrated packing models. In some cases in addition to showing the distribution histograms also a five-point smoothing was applied. For comparison, also "freshly cast" PTMSP was included for which hitherto only o-Ps accessible free volume distributions have been published.[4] In addition, for similar reasons, Figure 8 presents the data on the oxygen accessible free volume distributions for PTMSS (cf. ref 4); this is a conventional glassy polymer having $P(O_2)$ of only 56 barrers.[27] The results of the experimental probe methods are shown by the arrows in the *R*_max plots shown as Figure 7 and are also listed in Table 7.

In this regard, a comment should be made. Some of the probe methods (PALS, $^{129}$Xe/NMR) involve calculations of average hole size based on certain assumptions on their geometry. Thus, the classical PALS approach implies a spherical form of free volume elements with the radius that can be related to the longest positron annihilation lifetimes using the Tao−Eldrup formula.[36] It seems more likely that for polymers free volume elements have elongated shape and can be approximated by cylinders or ellipsoids. Accordingly, different equations have been proposed to relate the observed

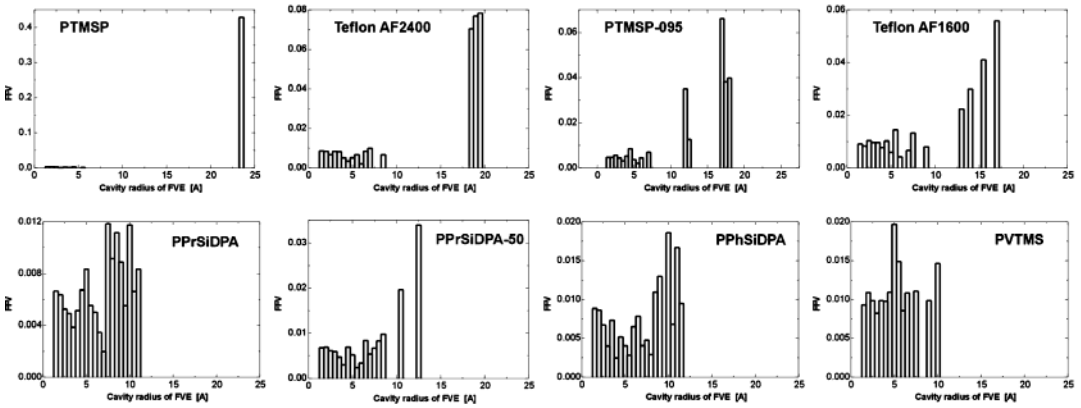


**Figure 6.** *V*_connect accessible free volume distributions for the positronium probe molecule ($R = 1.1$ Å).

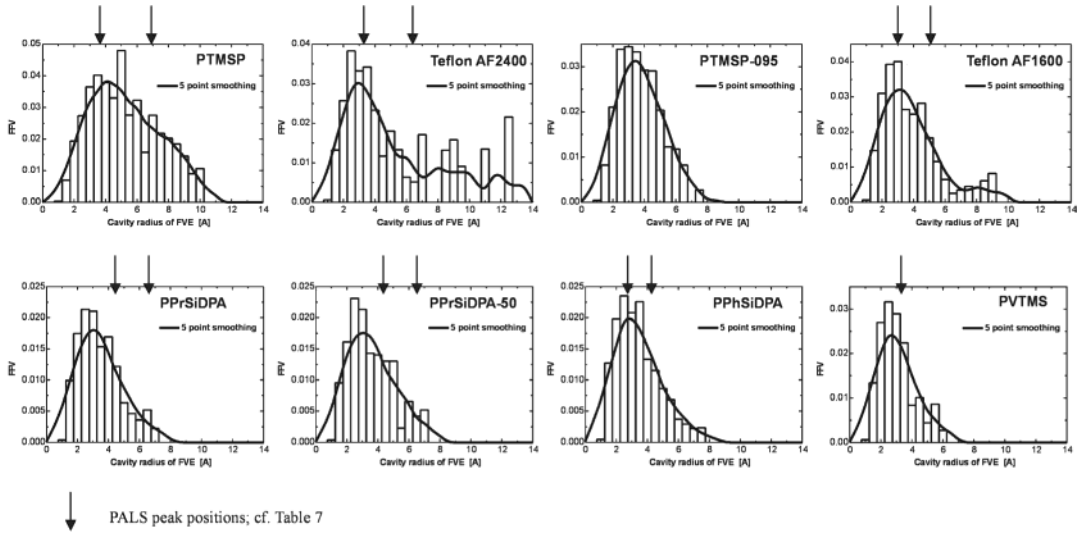


**Figure 7.** *R*_max accessible free volume distributions for the positronium probe molecule ($R = 1.1$ Å). The arrows indicate average PALS peak positions (cf. Table 7).

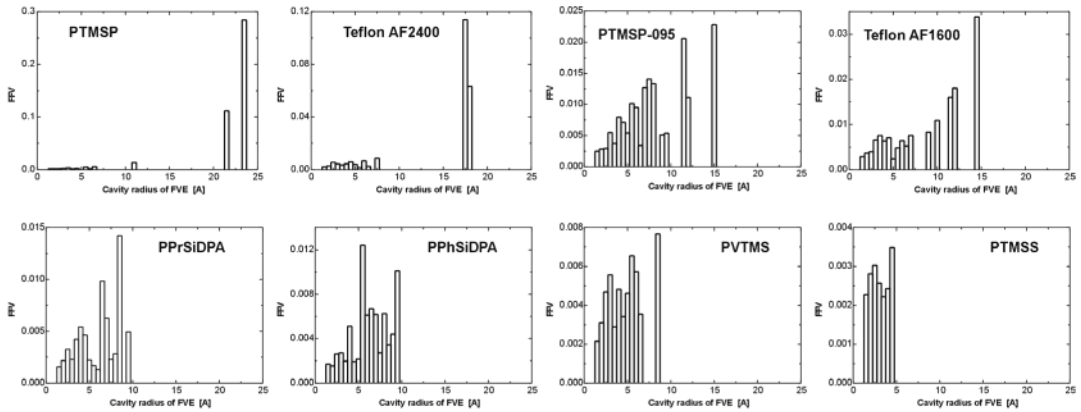


**Figure 8.** *V*_connect accessible free volume distributions for the oxygen probe molecule ($R = 1.73$ Å).

parameters (lifetimes in the PALS method and chemical shifts in the $^{129}$Xe/NMR method).[37,38] Recently, in another different computer simulation study[39] with contributions from one of the authors of the present paper (D.H.), it was shown (for a poly(amide imide) as an example) that a cigarlike average shape of free volume elements would be a much more appropriate assumption. This means that for example peak positions of FFV distributions obtained using the Tao−Eldrup model may be subject to a certain amount of systematic errors. It should also be mentioned that, in comparison to molecular modeling which considers all accessible free volume, PALS gives more weight to the larger holes in the distribution[36] because o-Ps tends to annihilate preferentially in these holes. That means that particularly for conventional glassy polymers with relatively small holes the FFV peak positions from the molecular modeling can be considerably lower than those based on the PALS results. For ultrahigh free volume polymers like PTMSP or AF2400, on the other hand, this discrepancy should be less pronounced.

Figures 6−8 present the results of hole size distributions obtained from packing models of various polymers considered in this work. The curves shown are averages over all packing models available for a given polymer. The following factors were analyzed: nature of poly-

**Table 7. Radii of Free Volume Elements (Å) Based on Various Probe Methods[15,17,18] [a]**

| | PALS | | | | $^{129}$Xe/NMR | | |
|---|---|---|---|---|---|---|---|
| | $R_{sp}$ | | $R_c$ | | | | |
| polymer | $R_3$ | $R_4$ | $R_3$ | $R_4$ | $R_{sp}$ | $R_c$ | IGC |
| PTMSP | 3.4 | 6.8 | 4.2 | 7.0 | 7.8 | 5.0 | |
| AF2400 | 2.7 | 6.0 | 3.7 | 6.3 | 6.7 | 4.4 | 6.4 |
| AF1600 | 2.5 | 4.9 | | 5.4 | | | 5.8 |
| PPrSiDPA | 3.8 | 6.4 | 4.5 | 6.6 | | | |
| PPhSiDPA | 2.4 | 3.8 | 3.4 | 4.5 | | | |
| PVTMS | 3.2 | 4.35 | 4.1 | 5.0 | | | 5.3 |

[a] $R_{sp}$ = data evaluation assuming spherical holes, $R_c$ = data evaluation assuming cylindrical holes, IGC = inverse gas chromatography.

mers, type of the topology of free volumes (*V*_connect vs *R*_max), size of a probe (o-Ps vs $O_2$).

The roles of these factors will be considered separately for high permeability and conventional glassy polymers. In the analysis of hole size distribution we will also address the results obtained using experimental probe methods (PALS, $^{129}$Xe/NMR, IGC) and, to some extent, the information on the transport properties of the polymes.

**4.3. High Permeability Polymers.** We assign to this group the polymers PTMSP and AF2400 together with the related materials PTMSP-095 and AF1600. Then the most important finding as revealed by Figure 6 is that in the *V*_connect approximation bimodal hole size distributions with a distinct gap between both modes are found for all these high permeability polymers. This feature is connected with the existence of two qualitatively different free volume phases: one composed of relatively small mostly disconnected holes like in conventional polymers and one with microvoids showing continuity in one direction. It should be mentioned that in the case of the aged PTMSP-095 the six investigated models showed a relatively large scatter (between 12 and 18 Å) of the peaks resulting from the respective continuous hole phase.

It should be remarked that the sizes of the packing models in the present work and in ref 4 are basically the same (47 ± 2 Å) for all four investigated high permeability polymers. Thus, it makes sense to compare the actual positions and magnitudes of the continuous hole phase *V*_connect peaks between the different high free volume polymers. (It should be, however, noticed that for a given polymer the positions of the FFV peaks for the continuous hole phase do of course depend on the respective model size. The reason is that although the assignment of individual holes in a model considers the periodic boundary conditions, the determined hole size distribution quantitatively only relates to the information available in the original packing cell of limited size; i.e., even if a model shows a clear presence of a continuous hole phase, the average dimensions determined from this phase via *V*_connect will be always considerably below the lateral length of the respective packing cell.) Considering the still relatively small size of the packing cells for the investigated high permeability polymers the position of the peaks in the higher radius area should show some correlation to the average lateral dimensions of the respective continuous hole phase. Thus, a qualitative comparison leads to the following sequence for this parameter (in decreasing order): PTMSP, AF2400, AF1600, PTMSP-095.

Another potentially interesting feature of the *V*_connect data shown in Figure 6 is that PTMSP has by far the highest percentage of free volume organized in the continuous hole phase. This is can be concluded from the area under the peak at about 23 Å, which indicates the continuous phase (and which would shift to higher values if even larger packing models would be used) and the area under the "conventional" peak in the lower radii range of about 1−5 Å. (This result is in good coincidence with PALS findings as for example shown in ref 4.) With this respect PTMSP is followed by AF2400, the (aged) PTMSP-095, and AF1600. This corresponds already in principle to the observed sequence of small gas molecule permeabilities in these materials (cf. Table 1).

The position of the *V*_connect peak for PTMSP at 23 Å shows a difference of about 4 Å to the results reported earlier[4] where this peak appeared at about 19 Å. This is caused by the improved correction of the size of an individual hole (cf. above). It should be noted, however, that this improved correction in comparison to the one utilized in ref 4 seems to cause no significant changes of *R*_max distributions in general (cf. e.g. respective data for PTMSP in Figure 7) and for *V*_connect distributions in the case of conventional polymers. Only the positions of the *V*_connect peaks related to a possible continuous hole phase are shifted by a few angstroms.

Here it shall be stressed that the *V*_connect distributions contain all the relevant topological information about the free volume of a polymer considering models of a given size. The *R*_max approach on the other hand is just a first attempt to partly reproduce the feature of PALS to not "see" large holes of complex topology as single entities but to split them in a number of more compact subholes (cf. Figure 5, right). With this regard it could be demonstrated in a foregoing paper[4] that the *R*_max FFV distributions can in some cases permit a better estimate about peak positions of FFV distributions obtained from experimental PALS data than the *V*_connect approach. The experimentally derived FFV intensity distributions on the other hand are often not well described for high permeability polymers with the *R*_max approach because it splits the continuous hole phase obviously in too many small holes; i.e., there is a bias for the intensity of the small radius peak in a bimodal distribution. It will be a task for the future to modify the *R*_max approach as to give an acceptable fit for both PALS determined FFV peak positions and intensity distributions. Then it would become clear how exactly PALS is splitting for example a continuous hole phase of a high permeability polymer in smaller subholes.

Figure 7 contains the data from the current *R*_max approach. There PTMSP, besides a "conventional" FFV distribution peak with a maximum at about 4 Å range, shows a distinct shoulder (indicating bimodality) in the 6−8 Å range. This corresponds reasonably well to experimentally obtained peak positions as shown in Table 7. The aged PTMSP-095 models on the other hand reveals a much narrower *R*_max distribution similar to those observed for conventional glassy polymers. It can be reminded that this is consistent with observations made thanks to application of the PALS method for investigations of PTMSP aging. There, it has been shown[23,44] via PALS that the aging of this polymer is accompanied by a reduction of hole size and, at least for the samples undergone some oxidation, by a shift from bimodal to monomodal hole size distribution. Here it should be mentioned again that the chosen density

of 0.95 g/cm$^3$ for the PTMSP-095 models corresponds to the case of very considerably aged PTMSP.

Both Figures 6 and 7 indicate that the Teflons AF2400 and AF1600 should at least show a bimodal distribution in PALS investigations with the first peak near 3 Å and the second (relatively wide) peak in the range between 6 and about 12 Å. This prediction is confirmed by PALS only for the first peak, while the second peak is measured at smaller radii (about 5 Å for AF1600 and about 6 Å for AF2400; cf. Table 7). Possible reasons for this discrepancy for these completely fluorinated polymers can be overinterpretation of the *R*_max approach in its present shape or methodical problems in measuring PALS lifetime spectra and converting them in size distributions.

It would be interesting to compare the *V*_connect and *R*_max modeling data not only with PALS hole sizes but also with corresponding PALS probabilities of finding polymers holes with certain radii. Unfortunately, the experimental probe methods meet with serious difficulties in attempts to estimate explicitly these probabilities. Thus, it has been shown[45] that intensities of lifetimes in the PAL spectra can often not serve as measures of corresponding hole concentrations. Some new ideas how hole size distributions can be found in porous sorbents have been addressed by Shantarovich et al.[46] Bearing in mind all this, computer-based atomistic simulations provide a unique opportunity to determine quantitatively hole size distributions in polymers.

**4.4. Conventional Glassy Polymers.** First the *V*_connect distributions of the positron accessible FFV shall be briefly described (cf. Figure 6). There the investigated more conventional polymers, PPhSiDPA, PPrSiDPA, PPrSiDPA-50, and PVTMS, as expected do not show a tendency toward a continuous hole phase. This corresponds to the result already found from the qualitative view in Figure 1. The only significant discrepancy to the PALS data (cf. Table 7) concerns the PPhSiDPA models which have a *V*_connect distribution very similar to PPrSiDPA. A similar result is obtained from the respective *R*_max distributions (cf. Figure 7).

In addition, the minor differences for the positron accessible *R*_max and *V*_connect distributions observed in Figures 6 and 7 between the 100% and 50% trans models for PPrSiDPA can probably be completely attributed to statistics effects (average over eight and just three frames for PPrSiDPA and PPrSiDPA-50, respectively).

Concerning their oxygen permeability, the consideration of the oxygen accessible FFV distributions (cf. Figure 8) permits to identify certain differences between the more conventional polymers. The polymer of this group with the fastest oxygen permeation, PPrSiDPA, like in the positronium probe molecule case (cf. Figure 6) reveals a clearly bimodal oxygen accessible FFV distribution. The slower polymers PVTMS and PTMSS, on the other hand, show less structured less wide distributions. Again as for the positronium probe molecule case PPhSiDPA has an oxygen accessible FFV distribution very similar to PPrSiDPA although the published oxygen permeability data for PPhSiDPA are much lower than for PPrSiDPA. Thus, PPhSiDPA seems to be the only exception from the trend otherwise observed in this study that the structure (mono- or bimodality) and width of the oxygen accessible *V*_connect distribution are to a reasonable extent correlated with the observed oxygen permeabilities. A possible reason could be the exceptionally high glass transition temperature (cf. Table 1) of PPhSiDPA as compared with PPrSiDPA and all other investigated polymers. As could be shown elsewhere,[7] constants of diffusion and permeabilities for polymers with very different glass transition temperatures can depend quite considerably not just on the free volume distribution of a polymer but also on its local chain mobility controlling the lifetime of diffusion channels. Other in this case less likely causes for the mentioned problem could be related with influences of residual solvent in the experimentally characterized PPhSiDPA or with the parametrization of the force field applied for the simulations.

As in all foregoing discussions, the 50% trans PPrSiDPA-50 models (not shown in Figure 8 to permit the display of PTMSS) do not show significant differences to the 100% trans case PPrSiDPA. This indicates again that obviously, at least as far as small molecule solubilities and free volume distributions are concerned, a wide variety of cis−trans ratios about the double bonds in the backbone of this polymer is possible also for the real material.

## 5. Summary

Molecular modeling of different glassy polymers including the most permeable materials like PTMSP, amorphous Teflons AF, and several conventional glassy polymers enabled us to obtain free volume size distributions. Extended equilibration procedures were necessary to obtain reasonable packing models for the polymers. The solubility part of the Gusev−Suter Monte Carlo method was utilized to show a reasonable agreement between simulated and measured solubility values for the model structures.

The free volume size distribution of the created model structures was analyzed using two geometrical approaches: one (*V*_connect containing all available topological information) that considers even large holes with complicated geometry as single entities and another one (*R*_max) that splits larger lengthy holes of complex geometry in smaller ones of more compact shape to come closer to the situation met with PALS. The results of simulations of free volume size distribution were compared with different experimental studies of free volume in polymers. The main findings of the free volume modeling are as follows.

Fractional accessible volumes (FAV) for probes of different size (0−1.7 Å) were calculated for all the polymers. It could be demonstrated that the overall FFV (probe radius 0 Å) shows the worst correlation with the measured gas permeabilities while the FAV for oxygen does already lead to a better correlation.

For several highly permeable polymer structures, the existence of a bimodal, in some cases partly continuous, free volume size distribution was confirmed. As the permeability of polymers decreases, the bimodal distribution steadily transforms to a monomodal hole size distribution which is characteristic for conventional glassy polymers.

In most cases the *R*_max approach gave reasonable coincidences with FFV peak positions from PALS data. Further development of the *R*_max approach will help to get a better insight into how positronium molecules probe the holes of ultrahigh free volume polymers like PTMSP or AF2400.

The contribution of larger holes to the overall free volume is the greatest for PTMSP followed by AF2400 and AF1600, which is exactly the order of decreasing of the measured gas permeabilities. Physical aging of PTMSP, according to computer modeling, should be accompanied by reduction of the hole sizes and steady transformation of the PALS detected FFV distribution from bimodal to monomodal. Also in most cases of the investigated more conventional polymers a general trend of correlation between the width of the free volume distribution and the observed gas permeabilities was detected.

The character of free volume size distribution does not change significantly when the size of the probe used in modeling was increased from 1.1 Å (o-Ps) to 1.7 Å ($O_2$).

**Acknowledgment.** We acknowledge that parts of the work were supported by the European Commission "Growth" Program, "PERMOD−Molecular modelling for the competitive molecular design of polymer materials with controlled permeability properties", Contract #G5RD-CT-2000-200, and by the INTAS−RFBR 97−1525 grant. We also thank Dr. A. Alentiev (A. V: Topchiev Institute, Moscow) for helpful discussions.

## References and Notes

(1) Shrader, D. M., Jean Y. C., Eds.; *Positron and Positronium Chemistry*; Elsevier: Amsterdam, 1988.
(2) Victor, J. G.; Torkelson, J. M. *Macromolecules* **1987**, *20*, 2241.
(3) Bondar, V. I.; Freeman, B. D.; Yampolskii, Yu. P. *Macromolecules* **1999**, *32*, 6163−6171.
(4) Hofmann, D.; Heuchel, M.; Yampolskii, Yu.; Khotimskii, V.; Shantarovich, V. *Macromolecules* **2002**, *35*, 2129−2140.
(5) Müller-Plathe, F. *Acta Polym.* **1994**, *45*, 259−293.
(6) Gusev, A. A.; Müller-Plathe, F.; van Gunsteren, W. F.; Suter, U. W. *Adv. Polym. Sci.* **1994**, *16*, 207−247.
(7) Hofmann, D.; Fritz, L.; Ulbrich, J.; Schepers, C.; Böhning, M. *Macromol. Theory Simul.* **2000**, *9*, 293−327.
(8) *Polymer User Guide, Amorphous Cell Section, Version 4.0.0p*+; Molecular Simulations Inc.: San Diego, CA, 1999.
(9) Heuchel, M.; Hofmann, D. *Desalination* **2002**, *144*, 67−72.
(10) Nagel, C.; Schmidtke, E.; Günther-Schade, K.; Hofmann, D.; Fritsch, D.; Strunskus, T.; Faupel, F. *Macromolecules* **2000**, *33*, 2242−2248.
(11) Sun, H.; Rigby, D. *Spectrochim. Acta* **1997**, *53A*, 1301−1323.
(12) Rigby, D.; Sun, H.; Eichinger, B. E. *Polym. Int.* **1997**, *44*, 311−330.
(13) *Polymer User Guide, Polymerizer Section, Version 400p*+; Molecular Simulations Inc.: San Diego, CA, 1999.
(14) Hofmann, D.; Fritz, L.; Ulbrich, J.; Paul, D. *Comput. Theory Polym. Sci.* **2000**, *10*, 419−436.
(15) Shantarovich, V. P.; Kevdina, I. B.; Yampolskii, Yu. P.; Alentiev, A. Yu. *Macromolecules* **2000**, *33*, 7453−7466.
(16) Yampolskii, Yu. P.; Korikov, A. P.; Shantarovich, V. P.; Nagai, K.; Freeman, B. D.; Masuda, T.; Teraguchi, M.; Kwak, G. *Macromolecules* **2001**, *34*, 1788−1796.
(17) Alentiev, A. Yu.; Shantarovich, V. P.; Merkel, T. C.; Bondar, V. I.; Freeman, B. D.; Yampolskii, Yu. P. *Macromolecules* **2002**, *35*, 9513−9522.
(18) Golemme, G.; Nagy, J. B.; Fonseca, A.; Algieri, C.; Yampolskii, Yu. *Polymer*, in press.
(19) Yampolskii, Yu.; Paterson, R. Solubility of gases in glassy polymers, IUPAC-NIST Solubility Data Series, V.70; *J. Phys. Chem. Ref. Data* **1999**, *28*, 1255−1451.
(20) Gusev, A. A.; Arizzi, S.; Suter, U. W. *J. Chem. Phys.* **1993**, *99*, 2221−2227.
(21) Gusev, A. A.; Suter, U. W. *J. Chem. Phys.* **1993**, *99*, 2228−2234.
(22) The gsnet/gsdif Gusev−Suter method version of Accelrys. Inc., San Diego, 1999.
(23) Yampolskii, Yu. P.; Shishatskii, S. M.; Shantorovich, V. P.; Antipov, E. M.; Kuzmin, N. N.; Rykov, S. V.; Khodjaeva, V. L.; Platé, N. A. *J. Appl. Polym. Sci.* **1993**, *48*, 1935−1944.
(24) Nagai, K.; Masuda, T.; Nakagawa, T.; Freeman, B. D.; Pinnau, I. *Prog. Polym. Sci.* **2001**, *26*, 721−798.
(25) Alentiev, A. Yu.; Yampolskii, Yu. P.; Shantarovich, V. P.; Nemser, S. M.; Platé, N. A. *J. Membr. Sci.* **1997**, *126*, 123−132.
(26) Paul, D. R.; Yampolskii, Yu. P. *Polymeric Gas Separation Membranes*; CRC Press: Boca Raton, FL, 1994; p 177.
(27) Khotimskii, V. S.; Filippova, V. G.; Bryantseva, I. S.; Bondar, V. I.; Shantarovich, V. P.; Yampolskii, Yu. P. *J. Appl. Polym. Sci.* **2000**, *78*, 1612−1620.
(28) Hirayama, Y.; Yoshinaga, T.; Kususki, Y.; Nonomiya, K.; Sakakibara, T.; Tamari, T. *J. Membr. Sci.* **1996**, *111*, 169−182.
(29) Bondi, A. *Physical Properties of Molecular Crystals, Liquids, and Glasses*; Wiley: New York, 1968.
(30) Merkel, T. C.; Bondar, V.; Nagai, K.; Freeman, B. D. *J. Polym. Sci., Part B: Polym. Phys.* **2000**, *38*, 273−296.
(31) Merkel, T. C.; Bondar, V.; Nagai, K.; Freeman, B. D.; Yampolskii, Yu. P. *Macromolecules* **1999**, *32*, 8427−8440.
(32) Nagel, C.; Günther-Schade, K.; Fritsch, D.; Srunskus, T.; Faupel, F. *Macromolecules* **2002**, *35*, 2071−2077.
(33) Alentiev, A.; Yampolskii, Yu. *J. Membr. Sci.* **2002**, *206*, 291−306.
(34) Ronova, I.; Rozhkov, E.; Alentiev, A.; Yampolskii, Yu. *Macromol. Theory Simul.*, in press.
(35) Teplyakov, V.; Meares, P. *Gas Sep. Purif.* **1990**, *4*, 66.
(36) Eldrup, M.; Lightbody, D.; Sherwood, J. N. *Chem. Phys.* **1981**, *63*, 51−58.
(37) Goworek, T.; Ciesielski, K.; Jasinska, B.; Wawzyszczuk, J. *Radiat. Phys. Chem.* **2000**, *58*, 719.
(38) Fraissard, J.; Ito, T. *Zeolites* **1988**, *8*, 354−358.
(39) Schmidtke, E.; Günther-Schade, K.; Hofmann, D.; Faupel, F. *J. Mol. Graphics*, submitted for publication.
(40) Yampolskii, Yu. P.; Shantarovich, V. P.; Chernyakovskii, F. P.; Kornilov, A. I.; Plate, N. A. *J. Appl. Polym. Sci.* **1993**, *47*, 85−92.
(41) Consolati, G.; Genco, I.; Pegoraro, M.; Zanderighi, L. *J. Polym. Sci., Part B: Polym. Phys.* **1996**, *34*, 357−367.
(42) Shantarovich, V. P.; Azamatova, Z. K.; Novikov, Yu. A.; Yampolskii, Yu. P. *Macromolecules* **1998**, *31*, 3963−3966.
(43) Consolati, G.; Rurali, R.; Stefanetti, M. *Chem. Phys.* **1998**, *237*, 493−499.
(44) Nagai, K.; Hill, A. J.; Freeman, B. D. *J. Polym. Sci., Part B: Polym. Phys.* **2000**, *38*, 1222−1239.
(45) Shantarovich, V. P.; Goldankii, V. I. *Hyperfine Interact.* **1998**, *116*, 67−81.
(46) Shantarovich, V. P.; Suzuki, T.; He, C.; Davankov, V. A.; Pastukhov, A. V.; Tsyurupa, M. P.; Kondo, K.; Ito, Y. *Macromolecules* **2002**, *35*, 9723−9729.
(47) Ichiraku, Y.; Stern, S. A.; Nakagawa, T. *J. Membr. Sci.* **1987**, *34*, 5−18.
(48) Plate, N. A.; Bokarev, A. K.; Kaliuzhnyi, E. G.; Litvinova, V. S.; Khotimskii, V. S.; Volkov, V. V.; Yampolskii, Yu. P. *J. Membr. Sci.* **1991**, *60*, 13−24.
(49) Kang, Y. S.; Shin, E. M.; Jung, B. M.; Kimm, J. J. *J. Appl. Polym. Sci.* **1994**, *53*, 317−323.
(50) Resnick, P. R.; Buck, W. H. In *Modern Fluoropolymers High Performance Polymers for Diverse Applications*; Scheirs, J., Ed.; John Wiley & Sons: New York, 1997; pp 397−419.
(51) Shishatskii, A. M.; Yampolskii, Yu. P.; Peinemann, K.-V. *J. Membr. Sci.* **1996**, *112*, 275−285.
(52) De Angelis, M. G.; Merkel, T. C.; Bondar, V. I.; Freeman, B. D.; Doghieri, F.; Sarti, G. C. *Macromolecules* **2002**, *35*, 1276−1288.

MA034971L